



## RESEARCH ARTICLE

# Cross-relaxation and temporal dynamics of lasing at 2 $\mu$ m in thulium-doped ceramic material

Alessandro Fregosi<sup>1</sup>, Fernando Brandi<sup>1</sup>, Luca Labate<sup>1</sup>, Federica Baffigi<sup>1</sup>, Gianluca Cellamare<sup>1</sup>, Mohamed Ezzat<sup>1</sup>, Daniele Palla<sup>1</sup>, Guido Toci<sup>2</sup>, Alex Whitehead<sup>1</sup>, and Leonida A. Gizzi<sup>1</sup>

### Abstract

We report the characterization of the pump absorption and emission dynamic properties of a Tm:  $Lu_2O_3$  ceramic lasing medium using a three-mirror folded laser cavity. We measured a slope efficiency of 73%, which allowed us to retrieve the cross-relaxation coefficient. The behavior of our system was modeled via a set of macroscopic rate equations in both the quasi continuous wave and the pulsed pumping regime. Numerical solutions were obtained, showing a good agreement with the experimental findings. The numerical solution also yielded a cross-relaxation coefficient in very good agreement with the measured one, showing that the cross-relaxation phenomenon approaches the maximum theoretical efficiency.

Keywords: high average power laser; ceramic laser materials; diode pumping; multipulse extraction; cross relaxation process

## 1. Introduction

The use of multi-TW ultrashort pulse lasers has been emerging dramatically in the past decades for fundamental studies and multidisciplinary applications<sup>[1]</sup>. Their effectiveness in exciting and driving plasma waves, for example, makes this class of lasers ideal as drivers of laser-plasma accelerators that are being considered for the next generation of compact light sources and are being investigated for future colliders for high-energy particle physics. The laser specifications in terms of repetition rate, and therefore average power, required for these applications are beyond current industrial capabilities, limited to a few tens of watts, with the most advanced scientific systems now in the 100 W range. Large, laser-based plasma accelerator infrastructures currently under construction<sup>[2-4]</sup> are based on PW-scale peak power lasers, with ultrashort pulse duration, down to 30 fs or less, and an energy per pulse up to 100 J, at a repetition rate for user applications up to 100 Hz and beyond. These projects rely on laser systems that are mostly based on Ti:sapphire, ideally with pump lasers featuring diode

pumping. However, the demanding specifications of pump lasers for Ti:sapphire, requiring nanosecond pulse duration and relatively short wavelength, limit the scalability of this technology.

Indeed, the possibility of scaling plasma acceleration further to meet particle physics needs<sup>[5]</sup> requires much higher efficiency, beyond the capabilities of most established technologies, thus calling for new solutions. A number of different approaches, based on entirely new concepts, materials and architectures, are being developed to overcome the fundamental limitations of present laser systems in terms of wall-plug efficiency, compactness and, ultimately, average power. Among these novel schemes, those based on thulium-doped materials lasing at 2 µm wavelength have been proposed as a promising ultrashort pulse laser platform with high average power and high repetition rate<sup>[6]</sup> for their potential high-energy storage capability<sup>[7]</sup>, mainly because of the long fluorescence time, of the order of milliseconds, and the convenient pumping wavelength, just below 800 nm. These features enable diode pumping with industrial-grade systems and also operation in the so-called multi-pulse extraction regime<sup>[8]</sup> at a very high repetition rate. Notably, 2 μm high-power high-repetition-rate laser systems with nanosecond pulse duration are currently being investigated as promising solid-state sources for improved extreme ultraviolet (EUV) lithography systems based on laser-driven tin microdroplet plasma emission<sup>[9–11]</sup>.

© The Author(s), 2025. Published by Cambridge University Press in association with Chinese Laser Press. This is an Open Access article, distributed under the terms of the Creative Commons Attribution licence (https://creativecommons.org/licenses/by/4.0), which permits unrestricted re-use, distribution and reproduction, provided the original article is properly cited.

<sup>&</sup>lt;sup>1</sup>Intense Laser Irradiation Laboratory (ILIL) Consiglio Nazionale delle Ricerche, Istituto Nazionale di Ottica (CNR-INO), Pisa, Italy

<sup>&</sup>lt;sup>2</sup>Consiglio Nazionale delle Ricerche, Istituto Nazionale di Ottica (CNR-INO), Sesto Fiorentino, Italy (Received 25 November 2024; revised 3 April 2025; accepted 17 April 2025)

Correspondence to: A. Fregosi, F. Brandi, and L. Labate, Consiglio Nazionale delle Ricerche, Istituto Nazionale di Ottica (CNR-INO), Via Moruzzi 1, Pisa 56124, Italy. Emails: alessandro.fregosi@ino.cnr.it (A. Fregosi); fernando.brandi@ino.cnr.it (F. Brandi); luca.labate@ino.cnr.it (L. Labate)

Recently, short pulse operation of thulium-doped vttrium lithium fluoride (Tm:YLF) has also been demonstrated<sup>[12]</sup> with TW-level peak power, confirming the potential of this platform. Thulium-doped polycrystalline ceramic materials are also being considered as gain media due to their high thermal conductivity, scalability, cost-effectiveness and doping flexibility<sup>[13]</sup>. Among those materials, ceramic Tm:Lu<sub>2</sub>O<sub>3</sub> along with other thulium-doped sesquioxides is being explored for their exceptional thermal conductivity, higher than that of any other laser material, which is suitable for relatively thick disk architectures<sup>[14,15]</sup>. In spite of the large quantum defect set by the 2 µm lasing wavelength, thulium-doped materials can exhibit efficient cross-relaxation (CR), a mechanism in which the energy of excitation, initially taken by one ion, is partially transferred to a neighboring ion originally in the electronic ground state, leaving both ions in the upper laser level<sup>[16]</sup>. While CR has been observed in thulium-doped materials, the extent to which this mechanism can be exploited remains an open issue, raising the need for a more extensive experimental investigation.

In this paper, we investigate the role of CR in polycrystalline ceramic Tm:Lu<sub>2</sub>O<sub>3</sub> with 4% (atomic fraction) doping, by considering the detailed steady-state dynamics and the accurate modeling of the pump and laser waist in the medium to carefully evaluate the absorbed laser energy. Our experimental results show that in our conditions CR is very efficient, with the coefficient approaching 1.9, leading to a slope efficiency well exceeding 70%.

# 2. Theoretical model for the Tm ion emission dynamics

In order to simulate the steady-state dynamics of the Tm:Lu<sub>2</sub>O<sub>3</sub> ceramic laser, we consider the energy levels and the transitions shown in Figure 1. The rate equations can be obtained from the ones in Ref. [17] as follows:

$$\frac{dN_4}{dt} = W_{14}N_1 - W_{41}N_4 - \frac{N_4}{\tau_4} - P_{41}N_4N_1 + P_{22}N_2^2, \quad (1)$$

$$\frac{dN_3}{dt} = -\frac{N_3}{\tau_3} + \frac{\beta_{43}N_4}{\tau_4}, \quad (2)$$

$$\frac{dN_2}{dt} = 2P_{41}N_4N_1 - 2P_{22}N_2^2 - \frac{N_2}{\tau_4} + \frac{\beta_{42}N_4}{\tau_4} + \frac{\beta_{32}N_3}{\tau_5}$$

$$\frac{dN_2}{dt} = 2P_{41}N_4N_1 - 2P_{22}N_2^2 - \frac{N_2}{\tau_2} + \frac{\beta_{42}N_4}{\tau_4} + \frac{\beta_{32}N_3}{\tau_3} + A_LN_1 - E_LN_2,$$
(3)

$$\frac{dN_1}{dt} = W_{41}N_4 - W_{14}N_1 + P_{22}N_2^2 - P_{41}N_4N_1 + \frac{N_2}{\tau_2} + \frac{\beta_{41}N_4}{\tau_4} + \frac{\beta_{31}N_3}{\tau_3} + E_LN_2 - A_LN_1,$$
(4)

where  $N_1$ ,  $N_2$ ,  $N_3$  and  $N_4$  are the population densities of the levels  ${}^3H_6$ ,  ${}^3F_4$ ,  ${}^3H_5$  and  ${}^3H_4$  respectively. The sum  $N_1 + N_2 + N_3 + N_4 = N$  is given by the total ion density, which can be inferred by the doping level. The spontaneous

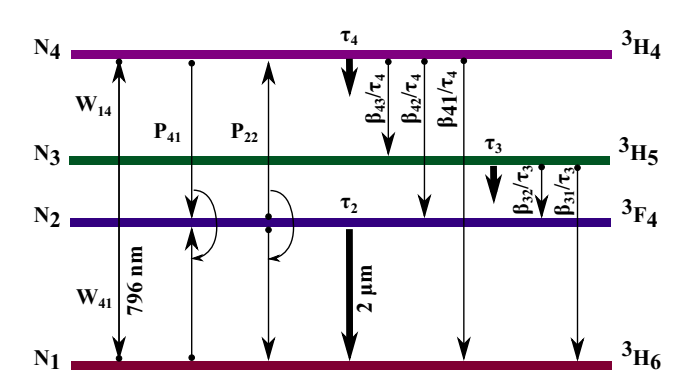


**Figure 1.** Scheme of the energy levels used to model the laser dynamics, drawn following the nomenclature used in Ref. [17].

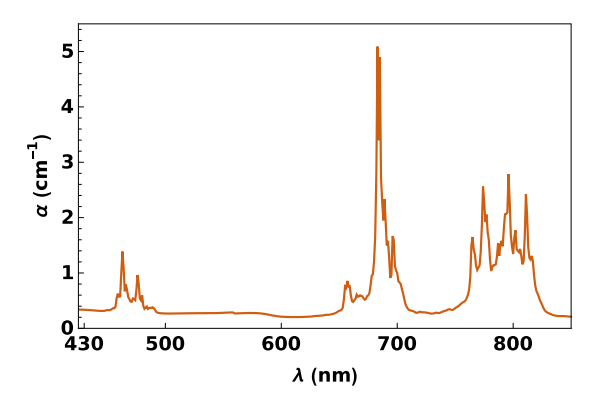


Figure 2. Measured absorption spectrum of the ceramic sample used in this work.

emission lifetime of the *i*-level is given by  $\tau_i$ , while  $\beta_{ij}$  represents the  $i \to j$ -level branching ratio, with  $\sum_j \beta_{ij} = 1$ . The pump rates are defined by  $W_{14}(t) = \sigma_a I_p(t)/h \nu_p$  and  $W_{41}(t) = \sigma_e I_p(t)/h \nu_p$ , where  $\sigma_a$  and  $\sigma_e$  are respectively the absorption and emission pump cross-section obtained from the measurements reported in Figure 2,  $I_p$  is the pump intensity, h is the Planck constant and  $\nu_p$  is the frequency of the pump laser. The functions  $E_L(t) = \sigma_{eL} I_L(t)/h \nu_L$  and  $A_L(t) = \sigma_{aL} I_L(t)/h \nu_L$  specify the lasing rates with  $\sigma_{aL}$  and  $\sigma_{eL}$  estimated from the data reported in Figure 7 shown later, which are similar to those found in Ref. [18]. Direct and inverse CRs are taken into account through the parameters  $P_{41}$  and  $P_{22}$ , respectively.

The systems of Equations (1)–(4) can be coupled with an optical cavity (modeled as a Fabry–Pérot resonator) by considering the equation obtained starting from<sup>[18]</sup>

$$\frac{\partial I_{L}(t)}{\partial t} = 2\left(\alpha_{L}(t)l - \frac{T}{2} - L\right) \frac{I_{L}(t) + I_{s}(t)}{T_{R}},\tag{5}$$

where  $\alpha_L = \sigma_{\rm eL} N_2 - \sigma_{\rm aL} N_1$  is the amplification coefficient, l is the medium thickness,  $T = 1 - R_1$  is the output coupler transmission and  $T_{\rm R} = l/c$  is the cavity roundtrip half time, where  $R_1$ ,  $R_2$  and D are the cavity mirror reflectivities and cavity length, respectively, and L represents the combined residual cavity losses. Equation (5) is

**Table 1.** Simulation parameters.

Symbol	Value
$\overline{R_1}$	0.97
$R_2$	0.999
L	0.013
$T_{ m R}$	0.40 ns
$\sigma_{ m a}$	$3.0 \times 10^{-25} \text{ m}^2$
$\sigma_{ m e}$	$8.3 \times 10^{-26} \text{ m}^2$
$\sigma_{ m aL}$	$8.4 \times 10^{-27} \text{ m}^2$
$\sigma_{ m eL}$	$4.2 \times 10^{-25} \text{ m}^2$
$w_0$	145 µm
$\Omega/4\pi$	0.0029

initialized by the spontaneous emission intensity term  $I_s(t) = N_2(t)h\nu_L l\Omega/(4\pi\tau_2)$ , with  $\Omega$  being the smaller solid angle defined by the mirrors and  $\nu_L$  the frequency of the emitted laser. The output laser intensity is given by  $I_{\text{out}}(t) = TI_L(t)$ .

The total Tm<sup>3+</sup> ion density with a doping percentage of  $\eta_{\rm d}$  (atomic fraction) is given by  $N(\eta_{\rm d}) = 2.8 \eta_{\rm d} \times 10^{28}~{\rm m}^{-3}$ where, in our case, we have  $\eta_d = 0.04$  ( $N = 1.12 \times 10^{27} \text{ m}^{-3}$ ). According to Refs. [17,19], we use  $\tau_i(\eta_d) = \tau_{i0}/(1 + A_i \eta_d^2)$ , where  $\tau_{20} = 3.4 \text{ ms}$  and  $\tau_{40} = 0.6 \text{ ms}^{[17,18,20]}$ . In our experimental conditions  $\tau_2(4\%) \simeq 1.22$  ms and  $\tau_4(4\%) \simeq 63$  µs, while  $\tau_3 \approx 2 \,\mu s$  is assumed to be independent of the dopant concentration. The branching ratio coefficients are given by  $\beta_{31} = 0.9793$ ,  $\beta_{32} = 0.0207$ ,  $\beta_{41} = 0.9035$ ,  $\beta_{42} = 0.0762$  and  $\beta_{43} = 0.0203^{[21]}$ . The CR mechanism is dominated by the direct  $P_{22}/P_{41} = 0.03 - 0.08^{[17,22,23]}$ . Following Ref. [22], the coefficient is given by  $P_{41}(\eta_d) = B\eta_d^2/(\eta_d^2 + \eta_0^2)$ , where  $\eta_0 = 4.3\%^{[24]}$  is the characteristic dopant concentration and  $B = 2.8 \times 10^{-22} \text{ m}^3 \text{ s}^{-1}$  is obtained from Refs. [22,23]. We find  $P_{41}(4\%) = 6.28 \times 10^{-29} \text{ m}^3 \text{ } \mu\text{s}^{-1}$ , with  $(P_{41}(4\%)N(4\%))^{-1} \simeq 14.2 \text{ }\mu\text{s}$ . The CR parameter  $\eta_{\text{CR}}$ can be numerically evaluated by considering the ratio  $\eta_{\rm CR} (P_{\rm eff}) = N_2/N_2^{\rm cr}$  under stationary conditions, where  $N_2^{\rm cr}$ are the results of the system of Equations (1)-(5) when the CR is forcefully turned off  $(P_{41} = P_{22} \equiv 0)$ . Above a certain threshold, which is approximately given by the lasing threshold of the system with no CR, the efficiency parameter becomes almost independent of the pump power and thus  $\eta_{\rm CR} (P_{\rm eff}) \rightarrow \eta_{\rm CR}$ .

Numerical simulations are performed considering a perfect overlapping between the pump and laser waist, so that the retrieved pump power actually corresponds to the effective absorbed pump power  $P_{\rm eff}$ . The slope efficiency is defined by  $\eta_{\rm sl} = P_{\rm out}/\left(P_{\rm eff} - P_{\rm eff}^{\rm th}\right)$ , where  $P_{\rm eff}^{\rm th}$  is the effective pump threshold. This value is related to  $\eta_{\rm CR}$  through  $\eta_{\rm sl} \simeq \eta_{\rm CR} \left(\lambda_{\rm P}/\lambda_{\rm L}\right) R_1/(R_1+L)$ , where  $\lambda_{\rm P}$  and  $\lambda_{\rm L}$  are the pump and laser wavelength, respectively. The limit is given by  $\eta_{\rm sl} \leq 0.8$  for  $\eta_{\rm CR} = 2$ . An alternative set of equations is considered in Ref. [18], where  $P_{\rm 4l} = P_{\rm 22} \equiv 0$ , while the measured  $\eta_{\rm CR}$  is directly introduced in Equation (5) by using  $\eta_{\rm CR}\sigma_{\rm eL}N_2 - \sigma_{\rm aL}N_1$  instead of  $\alpha_{\rm L}$ . The simulation parameters are reported in Table 1.

## 3. Experimental setup

The ceramic sample used in our study, with size 5 mm  $\times$  5 mm  $\times$  3.1 mm, was produced by Konoshima Chemicals Co., Japan.

As for its optical quality, the sample appeared transparent and clear. Its scattering coefficient was measured (using a p-polarized laser beam) in the visible region at a wavelength of 543 nm (where the Tm absorption is negligible). The overall transmission of the sample at the measurement wavelength was about 74%, to be compared to the theoretical value of 82% that can be calculated on the basis of the Fresnel reflection. Therefore, the losses determined by scattering on the ceramics defects were about 8%. Upon assuming an exponential law for the propagation into the sample, and by taking into account the reflection off the entrance and exit faces (uncoated) and the direction of propagation into the sample due to refraction, an absorption coefficient  $\alpha^{(543 \text{nm})} \simeq 0.3 \text{ cm}^{-1}$  can be retrieved.

Furthermore, a spectrophotometer was used to test the sample absorption at different wavelengths against known values. An example of such a measure is reported in Figure 2, and is in good agreement with those reported in the literature<sup>[18,20]</sup>. A set of similar measurements was performed at different transverse positions of the sample, which showed excellent sample transverse homogeneity.

In the measurements described here, the ceramic sample is mounted on a water cooled copper block. The thermal contact is ensured by a thin indium foil mounted between the lateral surface of the ceramic sample and the copper block itself. We use two working temperatures of 13°C and 23°C; the temperature is monitored by two one-wire sensors (Maxim, model DS18B20) with a 0.5°C sensitivity mounted on the sample holder.

Our test laser cavity is based on a three-mirror layout, as depicted in Figure 3, in a similar optical scheme to that in Ref. [25]; in particular, it features an end mirror (EM in Figure 3), through which the (longitudinal) pumping occurs, an output coupling mirror (OM) and a 100 mm curvature radius folding spherical mirror (SM). The pumping beam is obtained by a laser diode emitting at a measured wavelength of  $794.6 \pm 0.4$  nm, hence in the proximity of the absorption peak in Figure 2.

The laser diode is coupled to a multimode optical fiber of 200  $\mu$ m in diameter and a numerical aperture of 0.22. The beam emerging from the optical fiber is focused by two plano-convex f=50 mm optical doublets arranged in a 4f scheme. The  $M^2$  of the pump is measured using a similar procedure to that described, for instance, in Ref. [26]. The intensity profiles of the beam at several planes are found to be well fitted by a Gaussian function<sup>[27]</sup>; on applying a standard  $M^2$  corrected Gaussian propagation model to fit the observed widths as a function of the propagation distance, the beam waist is estimated to be  $w_P \simeq 160 \ \mu m$ , and  $M^2 \simeq 150$ ; this

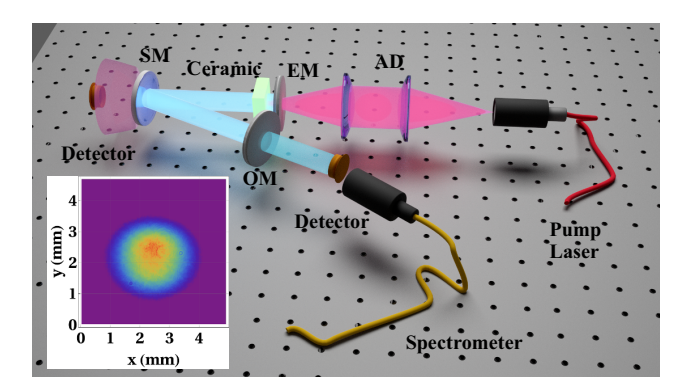


Figure 3. Scheme (not to scale) of the experimental apparatus: the achromatic doublets (ADs) are used to focus the pump beam from the optical fiber to the sample; the cavity is made up of three mirrors (see text); the dichroic entry mirror (EM) and the spherical mirror (SM) feature a high-reflectivity (HR) coating for approximately 2  $\mu$ m radiation and an anti-reflectivity (AR) coating for the pump wavelength. A 90% or 97% reflectivity output coupler mirror (OM) is used throughout the measurement. Both the pump and the laser beams are monitored in terms of power and spectrum with photodiodes, power meters and spectrometers. In the inset, the laser spot is captured at a distance of 500 mm from the output coupler mirror with a Dataray WinCamD camera.

is in rather good agreement (within 10%) with what can be estimated from theoretical considerations:  $M_{\text{(th)}}^2 \simeq 170$  (see, for instance, Ref. [28]).

We point out that, given the full width at half maximum of 2 nm of the pump diode laser emission, we did not observe any significant change in the behavior of the Tm:Lu<sub>2</sub>O<sub>3</sub> due to the slight detuning of the pump laser with respect to the exact absorption peak of 796.2 nm, except for a slight decrease in the radiation absorbed by the sample that is taken into account by the measurement procedure we used, which is described below.

We operate the pump laser with pulses lasting 10 ms repeated at a frequency of 10 Hz and we observe that the laser emission peaked at both 1965 and 2065 nm, as predicted in Refs. [20,29] and observed in Refs. [18,29]. In our case we observe only the 1965 nm wavelength emission when using the 90% reflectivity output coupler while using the 97% reflectivity output coupler and both emission wavelengths or just the 2065 nm one is visible, depending on the alignment of the cavity, and hence on the cavity losses; see Figure 4. All the data that are presented below in the text are taken with a well-aligned laser emitting only at 2065 nm.

## 4. Experimental results

We calculate the cavity beam size by means of the ABCD formalism<sup>[30]</sup>, obtaining a waist of  $144 \pm 5 \,\mu m$  roughly constantly across the ceramic sample.

Using the measured pump beam spot size and the laser beam model we can calculate the average pump rate  $\langle R_{\rm P} \rangle$  considering the volumetric overlap between the two beams

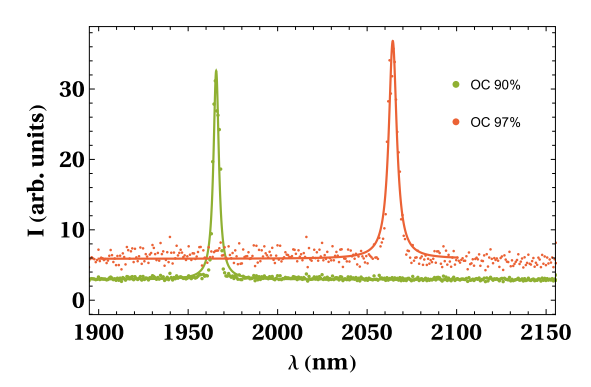


**Figure 4.** Laser spectra for the two 90% and 97% reflectivity output coupler mirrors. With the 97% reflectivity we observe a change in the emission spectra as a function of the cavity losses due to its alignment.

in the lasing medium<sup>[31]</sup>, as follows:

$$\langle R_{\rm p} \rangle = \frac{\alpha P_{\rm Inc}}{h \nu_{\rm p}} \frac{\int_0^d \frac{w_{\rm L}(z)^2}{w_{\rm L}(z)^2 + w_{\rm p}(z)^2} e^{-\alpha z} dz}{\frac{\pi}{2} \int_0^d w_{\rm L}(z)^2 dz},$$
 (6)

where  $P_{\text{inc}}$  is the pump laser power inside the sample. Assuming the laser beam has a constant spot size  $w_{\text{L}}$  inside the ceramic sample of length d we can calculate the effective absorbed pump laser power  $P_{\text{eff}}$  as follows:

$$P_{\rm eff} = \langle R_{\rm p} \rangle \pi w_{\rm L}^2 d = \chi P_{\rm inc}, \tag{7}$$

which in our case results in  $\chi = 0.47 \pm 0.06$ .

It is worth noting at this point the main limitations of the above procedure. Firstly, the laser beam profile inside the cavity is retrieved by the ABCD simulation; although this is a well-consolidated procedure in such experiments (see, for instance, Refs. [18,20]), it can result in some uncertainty. Secondly, Equation (7) holds in the case of a negligible depletion of the ground state of the medium, since the absorption coefficient considered could otherwise vary during laser operation. For this reason, we calculate the absorbed pump power as the difference between the power incident upon the active medium and the one transmitted through it. Since a direct measurement of the transmitted power directly downstream of the active medium (i.e., inside the cavity) would inhibit the lasing condition, making the procedure inconsistent, such a measurement is actually carried out using a silicon photodiode placed behind the SM (see Figure 3), in the direction of the pump beam; such a photodiode was preliminarily calibrated in order to retrieve an absolute figure for the transmitted pump power, under no lasing condition, using a power meter placed just after the active medium. Then, our actual measurements are carried out by simultaneously acquiring the laser power signal, using a power meter placed right at the exit of the cavity (behind the output coupler), and the absolutely calibrated photodiode signal from which the transmitted pump power

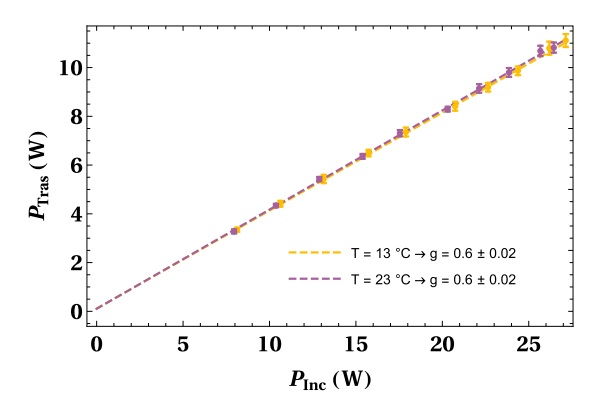


**Figure 5.** Pump laser power transmitted as a function of the incident pump laser power for the two different working temperatures of 13°C and 23°C. Straight lines are the results of a best fit calculation that we use to obtain the pump absorption ratio *g* in Equation (9).

can be retrieved. Finally we obtain the absorbed pump power as follows:

$$P_{\rm abs} = P_{\rm inc} - P_{\rm tras} \frac{V_{\rm on}}{V_{\rm off}},\tag{8}$$

where  $V_{\rm on}$  and  $V_{\rm off}$  refer to the photodiode signal with and without lasing, respectively, and considering as well the reflections at the ceramic faces. With this procedure, we observe a difference of up to 10% in the transmitted pump power with or without lasing. From the linear best fit to the data shown in Figure 5 we can observe that we always work below the saturation intensity; hence, the absorbed pump laser power can be written as follows:

$$P_{\text{tras}} = (1 - g)P_{\text{inc}},\tag{9}$$

resulting in  $g = 0.6 \pm 0.02$  in accordance with the fraction calculated using the small signal absorption coefficient  $\alpha = 322 \text{ m}^{-1}$ .

It should be noted that the value  $P_{\rm abs}$  we obtain with this procedure gives us the pump radiation absorbed over the whole volume described by the pump beam, which is larger than the laser beam; therefore, we calculate  $P_{\rm eff} = (\chi/g) P_{\rm abs}$ , which matches Equation (7) with the substitution  $P_{\rm abs} = g P_{\rm inc}$ .

The measured laser power as a function of  $P_{\rm eff}$  for the two working temperatures reported in Figure 6 shows a very small difference between the two datasets.

With our definition of  $P_{\rm eff}$  we obtain the slope efficiency of the laser by means of a best fit calculation of the experimental data in Figure 6 with the equation  $P_{\rm L} = m(P_{\rm eff} - P_{\rm thr})$  resulting in  $m_{13} = 0.75 \pm 0.02$  and  $m_{23} = 0.74 \pm 0.02$ , which gives CR parameters  $\eta_{\rm CR} = (\lambda_{\rm L}/\lambda_{\rm P}) \times m$  of 1.960.05 and 1.910.05, respectively, at 13°C and 23°C. We point out that these values are in agreement with values reported in the recent literature<sup>[18,20]</sup>, provided that the higher doping level of our sample and the dependence of  $\eta_{\rm CR}$  upon the Tm concentration given in Ref. [32] are taken into account.

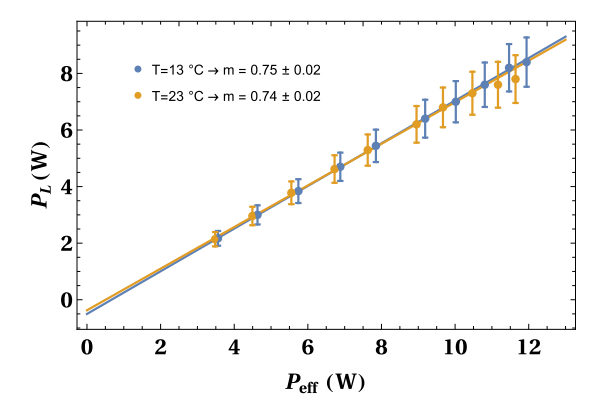


**Figure 6.** Laser power as a function of the effective absorbed pump power for the two working temperatures of 13°C and 23°C; the straight lines are the result of a best fit calculation that provides both the laser threshold power and the slope efficiency.

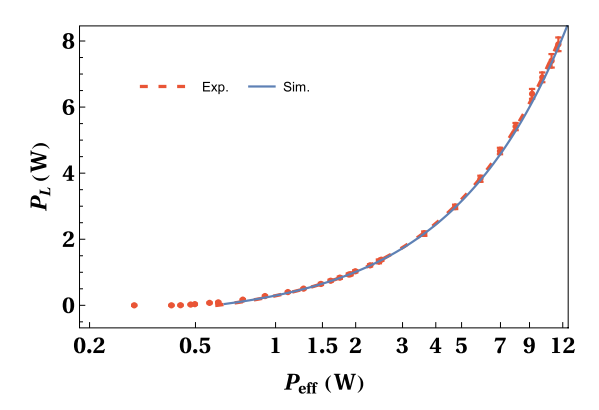


**Figure 7.** Experimental and theoretical laser power as a function of  $P_{\text{eff}}$ . The dashed line is a linear fit of the data, while the solid line is obtained with the model in Equations (1)–(5). The cavity energy loss L is tailored to 1.3% for the model to match the data.

To measure the laser threshold power we added to the apparatus a neutral density filter between the two lenses of the pump beam optics to obtain a lower pump laser power. The resulting laser power is reported in Figure 7 with the same best fit calculation resulting in a laser threshold of  $P_{\rm thr}=0.6\pm0.02$  W and in a slope efficiency  $m=0.73\pm0.02$  and a CR coefficient of  $\eta_{\rm CR}=1.89\pm0.05$  with a working temperature of 23°C. Data in Figure 7 are superimposed on the numerical simulation performed using the model described in Section 2, where the parameter L=1.1% results from the best fit on our data. The simulation results in a laser threshold of  $P_{\rm thr}=0.64$  W and a CR parameter  $\eta_{\rm CR}=1.91$ , in agreement with the experimental data.

To further validate the theoretical model we simulated the pulsed behavior of our system and compared the numerical results with the experimental one obtained by modulating the amplitude of the pump laser with rectangular pulses of tunable time duration at a fixed repetition frequency of 1 kHz. The data obtained are shown in Figure 8 superimposed to the simulation obtained using the term  $W_{41}$  in Equations (1)–(4) for the pump waveform recorded with a power calibrated silicon photodiode. The laser power is recorded with an

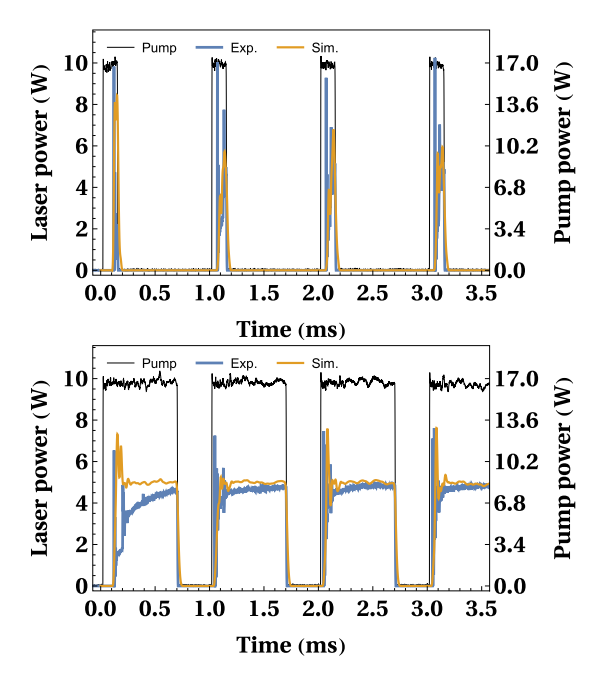


**Figure 8.** Experimental and theoretical laser power as a function of time obtained for pump pulse width of 150  $\mu s$  in the top panel and 700  $\mu s$  in the bottom panel.

indium gallium arsenide (InGaAs) photodiode and the signal obtained is scaled using the experimental slope efficiency of the laser. The raw data are filtered with a numerical low-pass filter with the cutoff frequency set at the sampling rate of the oscilloscope used to record the signals. In this case the pulsed dynamics of the laser intensity over a millisecond timescale is well reproduced by the simulation. As a matter of fact, the exact temporal dynamics at the rising edge of the pulse depends critically on the actual pump laser intensity rising profile, whose behavior over approximately 10 µs timescales is not perfectly captured by our experimental apparatus. Moreover, rather complex emission dynamics, possibly involving both the emission wavelengths reported above, was also experimentally observed in Ref. [18]; we are not accounting for this short timescale behavior, as it does not affect our comparison with the experimental data over the millisecond timescale considered in this paper. It is worth noticing that the delay asymptotically equal to 100 µs between the pump laser rising wavefront and the laser emission in the first pulse is independent of the pulse duration, while in the subsequent pulses, the delay is shorter but depends on time between the pulses. As a further remark, again from Figure 8 it can be noted that the laser emission amplitude reaches the steady state within the few initial pulses, that is, in a timescale comparable with the fluorescent time of the laser excited state  $\tau_{40}$ .

Finally, we can use the lifetime  $\tau_{40}$  of the excited manifold  $^3H_4$ , the  $P_{41}$  coefficient and thulium concentration N to calculate the CR coefficient. As reported  $^{[20,33]}$ ,  $\eta_{\rm CR} = \frac{P_{41}N}{1/\tau_{40}+P_{41}N}$  and, with our parameters, it results in  $\eta_{\rm CR} = 1.97$ , in good

agreement with our experimental and simulated values as well as with the values reported in the literature.

### 5. Conclusion

We investigated the lasing operations and characteristics of a ceramic sample of Tm:Lu<sub>2</sub>O<sub>3</sub> with 4% doping, using a threemirror test optical cavity. The observed laser efficiency of 73% at room temperature corresponds to a CR coefficient of approximately 1.9, in good agreement with the calculated value of 1.97. It is worth observing, at this point, that our measurements seem to point to a higher efficiency at lower gain medium temperatures, thus showing a way to further increase the efficiency of such a ceramic material; as a matter of fact, such an effect was recently reported in the literature for a similar material<sup>[34]</sup>, and tentatively explained via the more efficient depletion of the lower state involved in the laser transition. Furthermore, although not strictly related to the slope efficiency, we want to mention that in our experimental conditions the effective absorbed pump power is of the order of approximately 60%, and that this value can in principle be increased by suitable tweaks (for instance, increasing the length of the medium or allowing for a pump recirculation, or increasing the doping level), thus resulting in improved exploitation of the available pump power.

Finally, a numerical model of the laser dynamics, obtained by solving the macroscopic rate equations, is also presented here, and seen to reproduce with high accuracy the output laser power in both continuous and pulsed pumping regimes.

# Acknowledgements

The authors acknowledge the following funding: EU Horizon 2020 Research and Innovation Program EuPRAXIA Preparatory Phase, under Grant Agreement No. 101079773, EU Horizon IFAST, under Grant Agreement No. 101004730. This research has been co-funded by the European Union – NextGeneration EU 'Integrated infrastructure initiative in Photonic and Quantum Sciences' – I-PHOQS (IR0000016, ID D2B8D520, CUP B53C22001750006) and 'EuPRAXIA Advanced Photon Sources' – EuAPS (IR0000030, CUP I93C21000160006). We also acknowledge the contribution to the strategic view of this research by the Project 'Tuscany Health Ecosystem – THE' 'Spoke 1 – Advanced Radiotherapies and Diagnostics in Oncology' funded by the NextGenerationEU (PNRR), Codice progetto ECS000000017, D.D. MUR No. 1055 23 May 2022.

# References

C. N. Danson, C. Haefner, J. Bromage, T. Butcher, J. C. F. Chanteloup, E. A. Chowdhury, A. Galvanauskas, L. A. Gizzi, J. Hein, D. I. Hillier, N. W. Hopps, Y. Kato, E. A. Khazanov, R. Kodama, G. Korn, R. Li, Y. Li, J. Limpert, J. Ma, C. H.

- Nam, D. Neely, D. Papadopoulos, R. R. Penman, L. Qian, J. J. Rocca, A. A. Shaykin, C. W. Siders, C. Spindloe, S. Szatmári, R. M. G. M. Trines, J. Zhu, P. Zhu, and J. D. Zuegel, High Power Laser Sci. Eng. **7**, e54 (2019).
- 2. R. Assmann, M. K. Weikum, T. Akhter, D. Alesini, A. S. Alexandrova, M. P. Anania, N. E. Andreev, I. Andriyash, M. Artioli, A. Aschikhin, T. Audet, A. Bacci, I. F. Barna, S. Bartocci, A. Bayramian, A. Beaton, A. Beck, M. Bellaveglia, A. Beluze, A. Bernhard, A. Biagioni, S. Bielawski, F. G. Bisesto, A. Bonatto, L. Boulton, F. Brandi, R. Brinkmann, F. Briquez, F. Brottier, E. Bru, M. Buscher, B. Buonomo, M. H. Bussmann, G. Bussolino, P. Campana, S. Cantarella, K. Cassou, A. Chance, M. Chen, E. Chiadroni, A. Cianchi, F. Cioeta, J. A. Clarke, J. M. Cole, G. Costa, M. E. Couprie, J. Cowley, M. Croia, B. Cros, P. A. Crump, R. D'Arcy, G. Dattoli, A. Del Dotto, N. Delerue, M. Del Franco, P. Delinikolas, S. De Nicola, J. M. Dias, D. Di Giovenale, M. Diomede, E. Di Pasquale, G. Di Pirro, G. Di Raddo, U. Dorda, A. C. Erlandson, K. Ertel, A. Esposito, F. Falcoz, A. Falone, R. Fedele, A. F. Pousa, M. Ferrario, F. Filippi, J. Fils, G. Fiore, R. Fiorito, R. A. Fonseca, G. Franzini, M. Galimberti, A. Gallo, T. C. Galvin, A. Ghaith, A. Ghigo, D. Giove, A. Giribono, L. A. Gizzi, F. J. Gruner, A. F. Habib, C. Haefner, T. Heinemann, A. Helm, B. Hidding, B. J. Holzer, S. M. Hooker, T. Hosokai, M. Hubner, M. Ibison, S. Incremona, A. Irman, F. Iungo, F. J. Jafarinia, O. Jakobsson, D. A. Jaroszynski, S. Jaster-Merz, C. Joshi, M. Kaluza, M. Kando, O. S. Karger, S. Karsch, E. Khazanov, D. Khikhlukha, M. Kirchen, G. Kirwan, C. Kitegi, A. Knetsch, D. Kocon, P. Koester, O. S. Kononenko, G. Korn, I. Kostyukov, K. O. Kruchinin, L. Labate, C. Le Blanc, C. Lechner, P. Lee, W. Leemans, A. Lehrach, X. Li, Y. Li, V. Libov, A. Lifschitz, C. A. Lindstrom, V. Litvinenko, W. Lu, O. Lundh, A. R. Maier, V. Malka, G. G. Manahan, S. P. D. Mangles, A. Marcelli, B. Marchetti, O. Marcouille, A. Marocchino, F. Marteau, A. M. de la Ossa, J. L. Martins, P. D. Mason, F. Massimo, F. Mathieu, G. Maynard, Z. Mazzotta, S. Mironov, A. Y. Molodozhentsev, S. Morante, A. Mosnier, A. Mostacci, A. S. Muller, C. D. Murphy, Z. Najmudin, P. A. P. Nghiem, F. Nguyen, P. Niknejadi, A. Nutter, J. Osterhoff, D. O. Espinos, J. L. Paillard, D. N. Papadopoulos, B. Patrizi, R. Pattathil, L. Pellegrino, A. Petralia, V. Petrillo, L. Piersanti, M. A. Pocsai, K. Poder, R. Pompili, L. Pribyl, D. Pugacheva, B. A. Reagan, J. Resta-Lopez, R. Ricci, S. Romeo, M. R. Conti, A. R. Rossi, R. Rossmanith, U. Rotundo, E. Roussel, L. Sabbatini, P. Santangelo, G. Sarri, L. Schaper, P. Scherkl, U. Schramm, C. B. Schroeder, J. Scifo, L. Serafini, G. Sharma, Z. M. Sheng, V. Shpakov, C. W. Siders, L. O. Silva, T. Silva, C. Simon, C. Simon-Boisson, U. Sinha, E. Sistrunk, A. Specka, T. M. Spinka, A. Stecchi, A. Stella, F. Stellato, M. J. V. Streeter, A. Sutherland, E. N. Svystun, D. Symes, C. Szwaj, G. E. Tauscher, D. Terzani, G. Toci, P. Tomassini, R. Torres, D. Ullmann, C. Vaccarezza, M. Valleau, M. Vannini, A. Vannozzi, S. Vescovi, J. M. Vieira, F. Villa, C.-G. Wahlstrom, R. Walczak, P. A. Walker, K. Wang, A. Welsch, C. P. Welsch, S. M. Weng, S. M. Wiggins, J. Wolfenden, G. Xia, M. Yabashi, H. Zhang, Y. Zhao, J. Zhu, and A. Zigler, Eur. Phys. J. Spec. Top. 229, 3675
- 3. P. Mason, N. Stuart, J. Phillips, R. Heathcote, S. Buck, A. Wojtusiak, M. Galimberti, T. de Faria Pinto, S. Hawkes, S. Tomlinson, R. Pattathil, T. Butcher, C. Hernandez-Gomez, and J. Collier, in *Conference on Lasers and Electro-Optics Europe & European Quantum Electronics Conference* (IEEE, 2023).
- C. M. Werle, C. Braun, T. Eichner, T. Hülsenbusch, G. Palmer, and A. R. Maier, Opt. Express 31, 37437 (2023).
- E. Adli, W. An, N. Andreev, O. Apsimon, R. Assmann, J.-L. Babiegeon, R. Bingham, T. Blackburn, C. Brady, M.

- Bussmann, B. Carlsten, J. Chappell, J. B. B. Chen, S. Corde, L. Corner, B. Cowan, B. Cros, J. England, E. Esarey, R. Fonseca, B. Foster, S. Gessner, L. A. Gizzi, D. Gordon, E. Gschwendtner, A. Hartin, B. Hidding, M. Hogan, S. Hooker, T. Hughes, A. Kanareykin, S. Karsch, V. Khoze, P. Kumar, W. Leemans, F. Lemery, A. Li, R. Li, V. Libov, E. S. Link, M. Litos, G. Loisch, N. Lopes, O. Lundh, A. Lyapin, E. Marin, M. Marklund, T. Mehrling, P. Muggli, P. Musumeci, Z. Najmudin, U. Niedermayer, J. Osterhoff, M. Palmer, R. Pattathil, M. Peskin, P. Piot, J. Power, A. Pukhov, H. Ratcliffe, M. Riembau, V. Sanz, G. Sarri, Y. Saveliev, L. Schlachter, L. Schaper, N. Schoeneberger, C. Schroeder, S. Schroeder, D. Schulte, A. Seryi, S. Shchelkunov, C. Siders, E. Simakov, C. Simon-Boissen, M. Spannowsky, C. Swinson, A. Szczepkowicz, R. Tarkeshian, J. Thomas, J. Tian, J. Tilborg, P. Tomassini, V. Tsakanov, J.-L. Vay, J. Vieira, H. Vincenti, R. Walczak, D. Wang, S. Webb, G. White, G. Xia, H. Yamamoto, T. You, and I. Zagorodnov, arXiv:1901.10370 (2019).
- E. Sistrunk, D. A. Alessi, A. Bayramian, K. Chesnut, A. Erlandson, T. C. Galvin, D. Gibson, H. Nguyen, B. Reagan, K. Schaffers, C. W. Siders, T. Spinka, and C. Haefner, Proc. SPIE 11034, 1103407 (2019).
- I. Tamer, B. A. Reagan, T. Galvin, J. Galbraith, E. Sistrunk, A. Church, G. Huete, H. Neurath, and T. Spinka, Opt. Lett. 46, 5096 (2021).
- T. C. Galvin, A. Bayramian, K. D. Chesnut, A. Erlandson, C. W. Siders, E. Sistrunk, T. Spinka, and C. Haefner, Proc. SPIE 11033, 1103303 (2019).
- L. Behnke, R. Schupp, Z. Bouza, M. Bayraktar, Z. Mazzotta, R. Meijer, J. Sheil, S. Witte, W. Ubachs, R. Hoekstra, and O. O. Versolato, Opt. Express 29, 4475 (2021).
- L. Behnke, E. J. Salumbides, G. Göritz, Y. Mostafa, D. Engels, W. Ubachs, and O. Versolato, Opt. Express 31, 24142 (2023).
- Y. Mostafa, L. Behnke, D. J. Engels, Z. Bouza, J. Sheil, W. Ubachs, and O. O. Versolato, Appl. Phys. Lett. 123, 234101 (2023).
- I. Tamer, Z. Hubka, L. Kiani, J. Owens, A. Church, F. Batysta, T. Galvin, D. Willard, A. Yandow, J. Galbraith, D. Alessi, C. Harthcock, B. Hickman, C. Jackson, J. Nissen, S. Tardiff, H. Nguyen, E. Sistrunk, T. Spinka, and B. A. Reagan, Opt. Lett. 49, 1583 (2024).
- 13. V. Rastogi and S. Chaurasia, Photonics 11, 942 (2024).
- D. Palla, L. Labate, F. Baffigi, G. Cellamare, and L. A. Gizzi, Opt. Laser Technol. 156, 108524 (2022).
- G. Cellamare, L. Labate, F. Baffigi, D. Palla, and L. A. Gizzi, Proc. SPIE 11777, 117770K (2021).
- 16. R. C. Powell and G. Blasse, in *Luminescence and Energy Transfer* (Springer Berlin Heidelberg, 1980), pp. 43–96.
- A. Albalawi, S. Varas, A. Chiasera, H. Gebavi, W. Albalawi, W. Blanc, R. Balda, A. Lukowiak, M. Ferrari, and S. Taccheo, Opt. Mater. Express 7, 3760 (2017).
- 18. I. Baylam, F. Canbaz, and A. Sennaroglu, IEEE J. Sel. Top. Quantum Electron. 24, 1601208 (2018).
- H. Gebavi, D. Milanese, R. Balda, S. Chaussedent, M. Ferrari,
   J. Fernandez, and M. Ferraris, J. Phys. D: Appl. Phys. 43, 135104 (2010).
- P. Loiko, P. Koopmann, X. Mateos, V. Serres, J. S. Jambunathan, A. Lucianetti, T. Mocek, M. Aguiló, F. Díaz, U. Griebner, V. Petrov, and C. Kränkel, IEEE J. Sel. Top. Quantum Electron. 24, 1600713 (2018).
- O. L. Antipov, S. Y. Golovkin, O. N. Gorshkov, N. G. Zakharov, A. P. Zinov'ev, A. P. Kasatkin, M. V. Kruglova, M. O. Marychev, A. A. Novikov, N. V. Sakharov, and E. V. Chuprunov, Quantum Electron. 41, 863 (2011).
- 22. M. Tao, Q. Huang, T. Yu, P. Yang, W. Chen, and X. Ye, Proc. SPIE **8796**, 87961W (2013).

 M. Falconieri, A. Lanzi, G. Salvetti, and A. Toncelli, Opt. Mater. 7, 135 (1997).

- 24. G. Rustad and K. Stenersen, IEEE J. Quantum Electron. 32, 1645 (1996).
- Y. Feng, G. Toci, B. Patrizi, A. Pirri, Z. Hu, X. Chen, J. Wei, H. Pan, X. Li, X. Zhang, S. Su, M. Vannini, and J. Li, J. Am. Ceramic Soc. 103, 1819 (2020).
- 26. A. E. Siegman, in *DPSS (Diode Pumped Solid State) Lasers: Applications and Issues* (Optica Publishing Group, 1998), paper MQ1.
- P. F. Moulton, IEEE J. Quantum Electron. QE-21, 073505 (1985).

- 28. M. H. Griessmann, A. C. Martinez-Becerril, and J. S. Lundeen, Opt. Continuum **8**, 2 (2023).
- P. Koopmann, R. Peters, K. Petermann, and G. Huber, Appl. Phys. B 102, 19 (2011).
- 30. H. Kogelnik and T. Li, Appl. Opt. 5, 1550 (1966).
- 31. O. Svelto, *Principles of Lasers* (Springer US, 2010).
- 32. L. Zheng, H. Wu, L. Zhang, Y. Luo, G.-H. Pan, X.-J. Wang, Z. Hao, and J. Zhang, Ceramics International 49, 11060 (2023).
- 33. K. van Dalfsen, S. Aravazhi, C. Grivas, S. M. García-Blanco, and M. Pollnau, Opt. Lett. **39**, 4380 (2014).
- 34. Y. Du, T. Dai, H. Sun, H. Kang, H. Xia, J. Tian, X. Chen, and B. Yao, Crystals 11, 798 (2021).